

Delayed annihilation of antiprotons in helium gas

S.N. Nakamura, R.S. Hayano, M. Iwasaki, and K. Shigaki

Department of Physics and Meson Science Laboratory, University of Tokyo, Bunkyo-ku, Tokyo 113, Japan

E. Widmann and T. Yamazaki

Institute for Nuclear Study, University of Tokyo, Tanashi, Tokyo 188, Japan

H. Daniel, T. von Egidy, F.J. Hartmann, P. Hofmann* and Y.-S. Kim

Physik-Department, Technische Universität München, D-85747 Garching, Germany

J. Eades

CERN, CH-1211 Geneva 23, Switzerland

(Received 2 November 1993)

The delayed annihilation of antiprotons, which was recently discovered in liquid ${}^4\text{He}$ at KEK, has been studied at CERN in gas-phase ${}^4\text{He}$ and ${}^3\text{He}$. The annihilation time spectra in gas ${}^4\text{He}$ at various pressures were found to be similar to that for liquid ${}^4\text{He}$. The observed average lifetime in the region $t > 1 \mu\text{sec}$ for 3 atm ${}^4\text{He}$ was about $3.2 \mu\text{sec}$, while for 3 atm ${}^3\text{He}$ gas it was $2.8 \mu\text{sec}$, i.e., shorter by 15%. The time spectra show a growth-decay-type function, which is indicative of the presence of a series of metastable states. For ${}^4\text{He}$ and ${}^3\text{He}$ they have nearly identical shapes, differing only in the time scale by $(14 \pm 3)\%$. These observations are qualitatively consistent with the atomic model of $\bar{p}e^- \text{He}^{2+}$ proposed by Condo [Phys. Lett. **9**, 65 (1964)]. The time spectra were found to be sensitive to the presence of small amounts (as small as 20 ppm) of H_2 . No evidence was seen for delayed annihilation in gaseous Ne.

PACS number(s): 36.10.-k

I. INTRODUCTION

It was long believed that any negatively charged hadron stopped in matter would annihilate by nuclear absorption within 10^{-12} sec after the capture by an atom of the stopping substance (i.e., after exotic-atom formation). Contrary to this belief, it has been found that a small fraction (2–3 %) of π^- 's [1], K^- 's [2], and \bar{p} [3] stopped in liquid helium are trapped in metastable states and survive with average lifetimes of 10 nsec, 40 nsec, and $3 \mu\text{sec}$, respectively.

This metastability may be interpreted as a property of neutral exotic helium atoms $X^- e^- \text{He}^{2+}$, where the "exotic" particle X^- is bound in a state with large principal quantum number n and large orbital angular momentum l . Since the $E1$ transition energies are much less than the electron ionization energy (~ 25 eV), fast Auger transitions are not possible. Furthermore, the neutrality resulting from the continued presence of an electron in this system makes deexcitation via Stark mixing less probable. This explanation was first suggested by Condo [4] to explain the anomalous free-decay fractions of π^- and K^- in helium bubble chambers, and later studied theoretically by Russell [5], nearly two decades before the experimental observation (see Ref. [6] for historical

accounts). Ahlrichs *et al.* [7] calculated the energy levels and lifetimes of the antiprotonic helium atom using the Born-Oppenheimer approximation. Recently, further theoretical studies have been carried out by Yamazaki and Ohtsuki in the atomic picture [8] and by Shimamura [9] and by Greenland and Thürwächter [10] in the molecular picture. According to these calculations, a typical radiative lifetime of a metastable state is a few μsec and there should be a series of such states in a cascade. We would therefore expect that the overall survival time will be longer than a single-state lifetime, while the observed value in liquid helium is only $3 \mu\text{sec}$. One explanation of this discrepancy might be that these calculations were made for isolated $X^- e^- \text{He}^{2+}$ atoms and did not take interactions with neighboring atoms into account, so that strictly speaking the results only apply to very dilute media and not to liquid helium. There is no theory available regarding the effect of neighboring helium atoms on the metastability, although the interactions with the surroundings are known to be important usually in determining the eventual fate of exotic atoms. Furthermore, the calculations do not give annihilation time spectra, because this requires the knowledge of the initial level population $P(n, l)$ which has been little studied experimentally or theoretically. Experiments on low-density media are therefore essential if we wish to understand the structure and the behavior of an isolated $X^- e^- \text{He}^{2+}$ atom.

To this end, we need a monoenergetic antiproton beam of the lowest possible energy, because the range straggling (distribution of the stopping position) has to be

*Deceased.

minimized. We are therefore continuing our studies of the delayed annihilation of antiprotons in helium gas at the low energy antiproton ring (LEAR) of CERN, which provides a high-quality and low-momentum antiproton beam which can be stopped in low density gas at various conditions of temperature and pressure. The present paper reports many experimental procedures and results not presented in the short description of the experiment already published [11]. The achieved stopping distributions of \bar{p} in He gas of 1–10 atm pressure will be discussed in Sec. II together with other experimental details. We were able to measure the pressure and impurity dependence of the trapping time as well as the difference between ^4He and ^3He . Section III gives an overview on the data analysis, and in Sec. IV the results are presented. In Sec. V we discuss the experimental results and their implications.

II. EXPERIMENTAL METHOD

The experiment (PS205) was performed at the $M1$ beam line of LEAR, where a small fraction ($\sim 1\%$) of the 105 MeV/c \bar{p} beam was available parasitically. The experimental setup is shown in Fig. 1. We took data on pure ^4He and ^3He gas at different pressures at room tem-

perature, as well as on ^4He with controlled admixtures of H_2 , and on pure Ne.

A. \bar{p} stopping distribution

The \bar{p} beam momentum and its spread were $p = 105$ MeV/c (kinetic energy $T = 5.85$ MeV) and $\Delta p/p \leq 10^{-3}$, respectively. The typical beam intensity in the present experiment was $\sim 5 \times 10^3 \bar{p}/\text{sec}$.

The \bar{p} 's left the beam line vacuum through a 100 μm thick Be window [see Fig. 1(c)]. They were detected by a 100 μm thick plastic scintillation counter (B) (10 mm diameter) placed 3.5 cm downstream, and entered a target gas chamber through a Kapton window (25 μm thick, 2 cm in diameter), 4 cm downstream of B . The B counter is shown in detail in Fig. 1(d). A square piece of plastic scintillator ($3 \times 3 \text{ cm}^2$ NE 102A, 100 μm thick) was glued to a 3 cm wide and 5 mm thick Lucite light guide containing a 2 cm diameter beam hole. The arrangement allowed some overlap of scintillator and light guide so that the \bar{p} 's outside the hole were still detected by B , but stopped and annihilated in the Lucite. This permitted us to eliminate spurious delayed events resulting from prompt pions produced by undetected \bar{p} 's (see Sec. II E).

An additional degrader (50 μm Kapton) was placed halfway between the B counter and the entrance window to tune the \bar{p} stopping position in the gas target chamber. The gas target chamber was a cylindrical stainless steel container of 6 cm inner diameter and 18 cm length.

Downstream of B a ring-shaped plastic scintillator (A) was placed (an outer diameter of 30 mm and an inner diameter of 10 mm). It was used to eliminate \bar{p} 's which are too far off the beam axis. The A counter also served for beam steering and diagnostics. It was placed downstream of B so that \bar{p} annihilation in the aluminized mylar foil light shield around A did not cause spurious delayed events.

We used He gas at room temperature and at pressures between 1 and 10 atm. To stop \bar{p} 's in a gas target such as ours, a low energy beam with a narrow momentum spread is essential. To calculate the necessary thickness of degraders and to estimate the range straggling inside the gas target, we used a Monte Carlo program developed by one of the authors (M.I.) and the tables of Janni [12]. In the high energy region the program uses Ziegler's parametrization of the proton energy loss [13] to calculate the antiproton energy loss. Below 100 MeV/c, the energy loss of antiprotons is known to be different from that of protons (Barkas effect). It has been extrapolated for all materials by a fit to data from Andersen [14] and was included in the calculation in the energy range between 5 MeV and 1 MeV. Below 1 MeV, the energy loss is assumed to be a flat function of the energy, as recent experiments at LEAR indicate [15].

Table I gives the energy losses calculated for the setup described above, assuming no energy straggling. For the estimation of the range straggling, the energy straggling was calculated by evaluating the Vavilov distribution [16] with a sixth-order Runge-Kutta-Fehlberg method. Table II compares the calculated ranges with those mea-

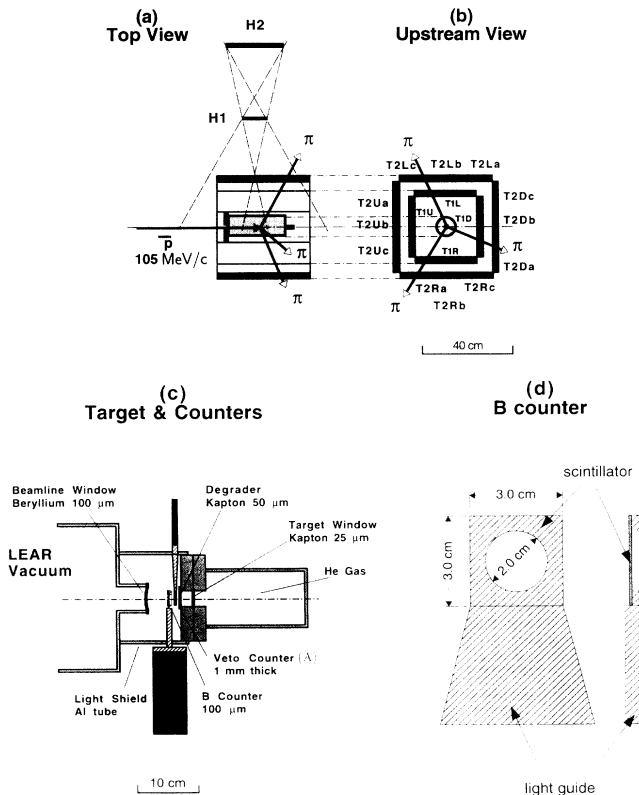


FIG. 1. Setup of the PS205 experiment. The top figures (a), (b) show the whole setup, and the lower parts (c), (d) the region around the beam counter. H denotes a hodoscope and T a telescope.

TABLE I. Calculated energy losses δT of \bar{p} 's in the windows and counters used in this experiment. x is the distance from the beamline window in beam direction, d the thickness of the material, d' the surface density of the material in mg/cm^2 , and T the kinetic energy of the \bar{p} 's after they traverse the material.

Location	Material	x (cm)	d	d' ($\frac{\text{mg}}{\text{cm}^2}$)	δT (MeV)	T (MeV)
Incident beam energy						
Beamline window	Be	0	100 μm	18.5	1.15	4.70
Gap	Air		3.5 cm	4.2	0.30	4.40
B counter	Plastic scintillator	3.5	100 μm	10.3	0.97	3.43
Gap	Air		2 cm	2.4	0.22	3.21
Degrader	Kapton	5.5	50 μm	7.0	0.77	2.44
Gap	Air		2 cm	2.4	0.28	2.16
Target window	Kapton	7.5	50 μm	3.5	0.50	1.66

sured by the hodoscopes (see Sec. II C). The errors of the calculation originate from uncertainties of the thicknesses of counters and windows (if the real thickness of the B counter differs by 10%, the range will shift by about 3 cm). Here the inclusion of the Barkas effect leads to a significantly larger range in the low density gas medium. The values calculated with the Barkas effect are still slightly smaller than the observed range, but taking into account the errors mentioned above, the agreement is satisfactory. With a 50 μm Kapton degrader, the \bar{p} 's were stopped in the center of the target vessel at a gas pressure of 3 atm. The calculated range straggling δR at 3 atm is about 4 cm [full width at half maximum (FWHM)], and at 10 atm about 1 cm. The experimental values for δR were obtained by unfolding the resolution (≈ 4.5 cm) of the hodoscopes. Since this resolution is of the same order as the straggling, the experimental values are not very accurate, but they agree with the results of the calculation.

In conclusion, for the 105 MeV/c \bar{p} beam, it is easy to achieve a stopping distribution of a few cm length along the beam axis even in a 1 atm gas target.

B. Gas handling and purification system

To ensure that the target gas we were using was sufficiently free of impurities, we proceeded very carefully in filling our gas chamber. As will be shown in Sec. IV, the purity of the gas turned out to be essential to observe the undisturbed lifetime of \bar{p} 's in He.

Our gas handling system consisted of gas bottles, sample cylinders, a molecular sieve, and a target vessel. The parts were connected by stainless steel pipes (1/4 in. diameter) and standard Swagelok joints. Target, sample

cylinders and molecular sieve could be evacuated separately by a turbo molecular pump. The target container was baked at about 200 $^{\circ}\text{C}$ for 2 h and evacuated before every gas change. Research grade ^4He or ^3He (impurity contents < 1 ppm) was passed through the molecular sieve cooled to 77 K to condense contaminations (mainly water). Needle valves were inserted between the molecular sieve and the gas bottle to control the gas flow into the target vessel.

C. Particle detection

To detect the charged annihilation products (π^{\pm}), we installed two counter systems. One was a hodoscope array (H1 and H2) used to measure the \bar{p} stopping position and covered only the small solid angle sufficient for this purpose. The other comprised four sets of telescope counters T_U , T_D , T_L , and T_R (for "Up," "Down," "Left," and "Right," respectively; see Fig. 1). The counters on either side consisted of one inner scintillator T1 and three outer scintillators T2a, T2b, and T2c. The telescope counters covered a total solid angle of 2π .

D. Time spectra

The time interval measured in the experiment is the delay between the passage of the beam antiproton through the B counter and the arrival of its annihilation products (π^{\pm}) in the T2 counters. A multistop long-range time to digital converter (LeCroy TDC Model 4208) was employed to measure this time interval, with its time gate (maximum time interval) set to 50 μsec . The multistop capability of the TDC Model 4208 was used to reject

TABLE II. Calculated and measured values for range and range straggling in helium gas of different pressure. δR is the full width at half maximum.

Pressure	3 atm		10 atm	
	$\langle R \rangle$ (cm)	δR (cm)	$\langle R \rangle$ (cm)	δR (cm)
Standard calculation	9.0 ± 2.0	3.8	2.7 ± 1.5	1.2
with Barkas effect	11.9 ± 2.0	3.8	3.6 ± 1.5	1.2
Experiment	13.5 ± 1.0	3 ± 1	6.6 ± 1.0	≈ 1

post-pileup events. We took a separate TDC spectrum for each of the outer 12 telescopes $T2_{\alpha\beta}$. The background rejection method will be described below. Antiprotons with 1.5 MeV energy need roughly 25 nsec to stop in 1 atm He gas. Soon after they are captured by He atoms and usually annihilate within 10^{-12} sec. The stopping-time distribution for these *prompt* annihilations is much shorter than our time resolution which is about 3 nsec. Thus our time spectra always contain a sharp peak corresponding to the *prompt* annihilations. In all spectra presented here, we define the annihilation time as the difference between the measured time interval and the prompt peak (the value $t = 0$ thus being assigned to the prompt peak).

E. Spurious events

Many spurious delayed events are created by the prompt annihilation of a second antiproton arriving within the observation time window (50 μ sec), while genuine delayed annihilation amounts to only 3% of the stopped antiprotons in liquid helium [3]. The average interval between two successive antiprotons at a typical beam flux of 5×10^3 \bar{p} /sec is thus comparable to our time window and can be expected to produce these spurious delayed events at a rate of about 25% of incoming \bar{p} . It is therefore essential to reject these events.

Figure 2 explains the different types of real and fake events which can occur in this experiment. The upper part shows a typical time distribution of incoming antiprotons, and the middle part a sequence of observed annihilation products (π^\pm). The lower part shows schematically the gate signal generated by the electronics, which is started by the detection of an antiproton (B counter hit) and stopped by the pion arrival (hit in one of the $T2$ counters). The length of this signal corresponds to the annihilation time. Typical events which may occur are listed below.

(a) *Prompt event (good event)*: most \bar{p} 's annihilate immediately, and prompt pions are observed.

(b) *Delayed event (good event)*: this is an event we are interested in. A \bar{p} is detected without any prompt pion signal, and some time later a delayed pion is observed.

(c) *Postpileup event (spurious delayed event, to be rejected)*: after a \bar{p} without an accompanying prompt pion was detected, the second \bar{p} arrives within the time window. In this case, we cannot tell which \bar{p} created an observed "delayed" pion. These so-called *post-pileup* events must be rejected. Most of the rejected events are from the prompt annihilation caused by the second \bar{p} .

(d) *Prepileup event (to be rejected)*: a good event as in (b) was detected, but within the observation time window of 50 μ s before the arrival of the \bar{p} , another \bar{p} is detected. This case occurs when the first \bar{p} did not make a trigger due to computer veto, but the second did. Again, the ambiguity of which \bar{p} corresponds to the pion makes it necessary to reject these *prepileup* events.

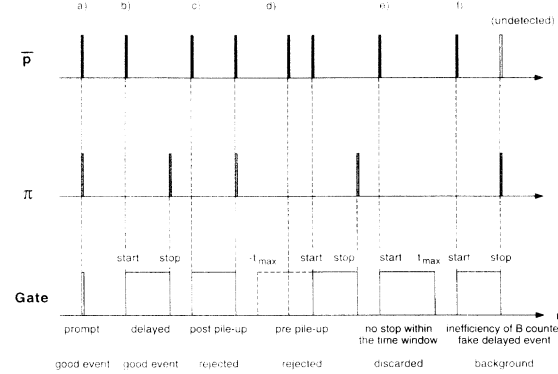


FIG. 2. Schematic diagram of the time distribution of typical events. For details see text.

(e) *Event loss*: a \bar{p} arrived, but within the time window no pion is detected. This will not be recorded.

(f) *Background*: after a \bar{p} without prompt pion was detected, a second \bar{p} arrives at the B counter, which inevitably does not have 100% efficiency. A prompt pion resulting from this second \bar{p} appears to be due to a real delayed event and is recorded. These spurious delayed events lead to a time-independent background in the annihilation time spectrum. This can only be strongly reduced by ensuring a high B counter efficiency. Removal of these spurious delayed events is a crucial element in achieving successful detection of the delayed annihilation of a small \bar{p} fraction. In the case of our B counter the inefficiency for 105 MeV/c antiprotons was estimated to be less than 0.1% from the background level for the empty target.

There exists another source for spurious delayed annihilation events, namely $\pi^+ \rightarrow \mu^+ \rightarrow e^+$ decays from positive pions stopped in the vicinity of the target. Since we have no particle identification system for the $T1$ counters, we cannot distinguish e^+ hits from π^\pm hits. This background is time-distributed according to the muon lifetime (2.2 μ sec), which lies within the time scale we are interested in. In order to remove this background, it is very effective to tag a multipion hit at the telescope counters, because only an antiproton annihilation will create more than one charged pion at the same time (the average multiplicity of π^\pm for \bar{p} ^4He reaction is approximately 3). The multipion tagging will be described in the following section.

We divided the $T2$ counters into 12 elements to reduce the probability of two pions hitting the same telescope counter (see Fig. 1). Thus a multiplicity cut can be applied without large loss of statistics.

F. Trigger condition and data acquisition

The trigger condition was as follows:

$$B * \bar{A} * \sum_{\alpha=\{U,R,D,L\}} \left(T1_\alpha * \sum_{\beta=\{a,b,c\}} T2_{\alpha\beta} \right) * \overline{\text{computer busy}} * \overline{\text{prepileup}}.$$

where * refers to “and” and the overbar refers to “not.” The hodoscopes $H1$ and $H2$ were only used to monitor the \bar{p} stopping position. A typical trigger rate was 2 kHz at the intensity of $10^4 \bar{p}/\text{sec}$.

Prepileup \bar{p} events were rejected in the trigger level by hardware. For the rejection of postpileup events, we took advantage of the multiple-stop recording capability of the TDC LeCroy Model 4208. We recorded the B -counter TDC information as well as that from the telescope counters. When the B -counter TDC was confronted with multiple stops (which means a second \bar{p} arrived within the time window), the event was rejected.

For each event, the TDC information as well as the corresponding hit pattern showing which of the telescope or hodoscope counters detected the particle, were recorded. The data were acquired by a CES-J11 (PDP-11 compatible CAMAC Auxiliary Controller) and were transferred to a VAX computer station through the Kinetics K3922-2922 Q-Bus controller using Direct Memory Access and then written on an 8 mm VCR tape. The dead time of the CES-J11 was typically $32 \mu\text{sec}$ per event. However, we have a $50 \mu\text{sec}$ time gate for the prepileup window as well as for the observation-time window, resulting in a dead time of $100 \mu\text{sec}$ per accepted event.

III. DATA ANALYSIS

The data analysis consisted of the following steps: (1) postpileup rejection (prepileup events had already been rejected); (2) adjustment of the time zero in the time spectra of all $T2$ counters; and (3) selection of events with simultaneous multipion hits.

Postpileup rejection was carried out by discarding any event with a second hit in the beam counters' TDC spectra (cf. Sec. II F). The time zero was reassigned to the most frequent value (prompt peak) every 1000 records on tape to eliminate electronic drifts. A time resolution of 2.3 nsec (equals FWHM of the prompt peak) was achieved.

To select coincidence hits in the telescope counters, we proceeded as follows: for each event, the average hit time $\langle t \rangle$ as well as the deviation Δ from $\langle t \rangle$ were calculated for all TDC's which contained valid time information;

$$\langle t \rangle = \frac{\sum_{\text{hit}} T_i}{N_{\text{hit}}}, \quad \Delta = \sqrt{\frac{\sum_{\text{hit}} (T_i)^2}{N_{\text{hit}}} - \langle t \rangle^2},$$

where N_{hit} refers to the number of TDC channels with valid time information.

Figure 3 shows the distribution of Δ in a run with an empty target, the antiprotons then stopping in the stainless steel target wall. Coincident T counter hits were accepted in the off-line analysis only when their value Δ was smaller than 3.3 nsec. Setting this threshold at 2.25 nsec did not change the quality and shape of the time distribution but only the statistics.

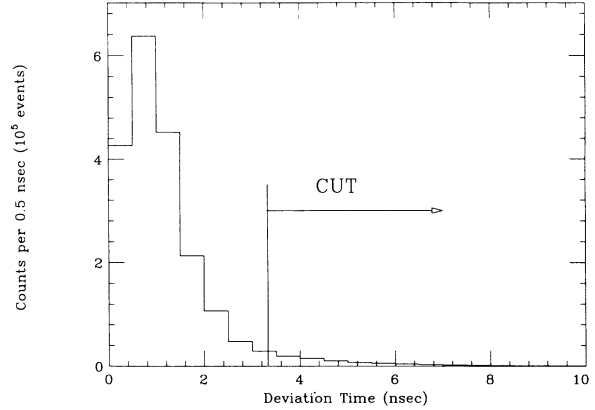


FIG. 3. Deviation of T-counter hit timing from the average timing in a typical run.

Figure 4 shows the effect of pileup rejection as well as $\geq 2\pi$ and $\geq 3\pi$ tagging. In Fig. 4 (a), the raw time spectrum is displayed. The large number of pileup events is drastically reduced by applying postpileup rejection [Fig. 4 (b)]. However, Fig. 4 (b) has an exponential delayed component with a lifetime of about $2.2 \mu\text{sec}$. This component is caused by $\pi^+ \rightarrow \mu^+ \rightarrow e^+$ decays as mentioned above and can be seen even in the time spectrum with 2π tagging [Fig. 4 (c)]. It is strongly suppressed by the 3π tagging [Fig. 4 (d)]. Therefore, a multiplicity of three charged particles in the telescope counters was required for the final time spectra.

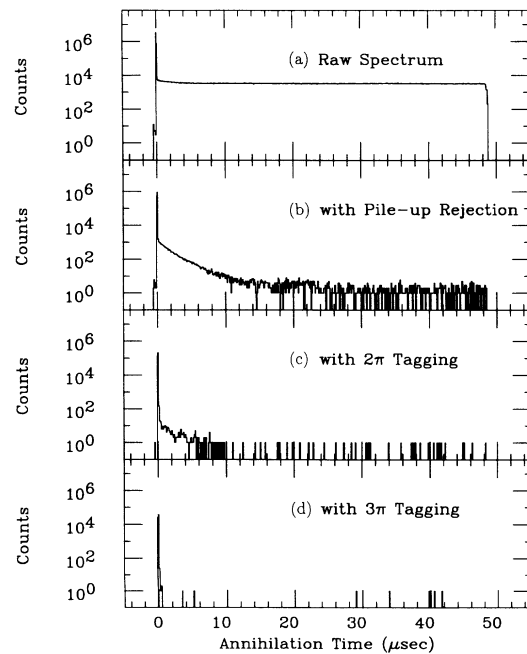


FIG. 4. Time spectra for an empty target: (a) raw data, (b) data after pileup rejection, (c) with additional $\geq 2\pi$ tag, and (d) $\geq 3\pi$ tag. For all figures, 100 nsec per channel binning was chosen.

IV. RESULTS

A summary of the data taken with all gas samples we used in this experiment is given in Table III. Figure 5 shows the final time spectra for the pure-He targets, the previous KEK results on liquid ^4He [3], and the pure Ne target. The overall shape of the time distribution of \bar{p} annihilation in helium is very similar for gases and liquid: namely, (1) the average lifetime is of the order of 3 μsec , and (2) the trapping fraction, i.e., the fraction of delayed to prompt events, is about 3%. On closer inspection, however, a systematic change in the shape of the region immediately following the prompt peak can be seen. This part becomes significantly steeper when going from low pressure gas to liquid.

Figure 6 shows the time spectra of ^4He and ^3He at a pressure of 3 atm, overlaid in the same figure. For better comparison, a binning of 500 nsec per channel has been chosen and the two spectra have been normalized to the number of accepted antiprotons. A first observation in these coarse binning spectra is that the shape of the delayed part is not purely exponential. Both spectra are bent *downwards* at $t > 10 \mu\text{sec}$, suggesting the presence of metastable states in the decay chain. Secondly, it is clearly seen that the lifetime of ^3He is shorter than that of ^4He and also that the trapping fraction is smaller.

In order to describe the spectra with a model independent parameter, let us define a local lifetime in a purely mathematical way. The observed annihilation time spectra were described by a function such as

$$N(t) = N_0 \exp[-f(t)] + \text{const}, \quad (1)$$

where $N(t)$ refers to the yield and $f(t)$ is a function of t . We can define the local lifetime (T_{local}) as follows:

$$T_{\text{local}}(t) = 1/f'(t). \quad (2)$$

The inset in Fig. 6 shows the local lifetime for typical conditions. It is clearly seen that the time spectra deviate significantly from a simple sum of exponential functions which would give an increasing T_{local} .

To represent the time spectra by a single value, we introduce the average lifetime $T_{\text{av}}(t_0, t_{\text{max}})$,

$$T_{\text{av}}(t_0, t_{\text{max}}) = \frac{\int_{t_0}^{t_{\text{max}}} tN(t)dt}{\int_{t_0}^{t_{\text{max}}} N(t)dt} - t_0. \quad (3)$$

TABLE III. Summary of all gas samples with the values for average lifetime [Eq. (3)] and trapping fraction [Eq. (4)].

Gas	Pressure	Impurity	$T_{\text{av}}(\mu\text{sec})$			$f_{\text{trap}}(\%)$
			($t_0 = 100 \text{ nsec}$)	(1 μsec)	(10 μsec)	
^4He	3 atm		3.08 ± 0.03	3.18 ± 0.04	2.69 ± 0.44	3.3 ± 0.2
^4He	5 atm		2.38 ± 0.04	2.70 ± 0.06	2.35 ± 0.94	3.1 ± 0.2
^4He	10 atm		2.49 ± 0.03	2.97 ± 0.04	2.99 ± 0.56	3.0 ± 0.2
^3He	2 atm		2.37 ± 0.02	2.62 ± 0.04	2.58 ± 0.84	2.6 ± 0.2
^3He	3 atm		2.49 ± 0.02	2.77 ± 0.03	2.26 ± 0.58	2.6 ± 0.2
Ne	2 atm					
^4He	6 atm	H ₂ 20 ppm	1.42 ± 0.02	1.99 ± 0.05		3.1 ± 0.2
^4He	6 atm	H ₂ 400 ppm	0.36 ± 0.02	1.85 ± 0.34		2.8 ± 0.2

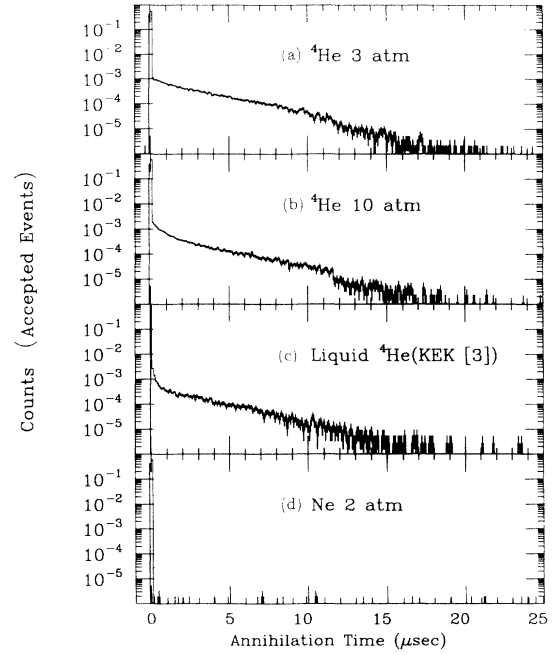


FIG. 5. Comparison of the time spectra of (a) ^4He gas at 3 atm and (b) 10 atm pressure with (c) data taken on liquid ^4He at KEK [3] and (d) Ne. Binning is 100 nsec per channel. Note the change in the shape of time distribution immediately following the prompt peak.

In the case that $N(t)$ is a single exponential function with lifetime τ and t_{max} is large compared with t_0 and τ , T_{av} becomes equal to τ . t_{max} was fixed to 50 μsec , our observation time. The observed time spectrum decreases steadily. Thus the region of small t has a larger weight in T_{av} . This means that if we make t_0 smaller, T_{av} reflects the behavior of the shorter lifetime components, while if t_0 goes to larger values, T_{av} reveals the presence of the longer lifetime components.

Table III summarizes the values of average lifetimes T_{av} and trapping fraction f_{trap} for each experimental condition. Here, we have assigned the events in the region $t < 20 \text{ nsec}$ as prompt and the remainder as delayed annihilations. Thus the trapping fraction is

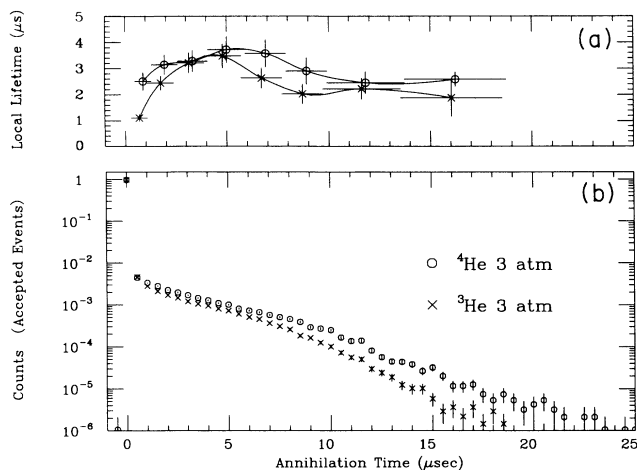


FIG. 6. Comparison of the local lifetimes (a) and time spectra (b) of ^4He at 3 atm and ^3He at 3 atm pressure. To exhibit the global structure of the figures, 500 nsec per channel binning was chosen. Note that the shape of the time spectra cannot be described by a single exponential function.

$$f_{\text{trap}} = \frac{N(20 \text{ nsec} < t < 50 \text{ } \mu\text{sec})}{N_{\text{total}}}. \quad (4)$$

For 3–10 atm pressure ^4He gases, the pressure dependence of the trapping fraction is not large. We may note here that at low pressure (< 500 mbar), it has been reported by others that the trapping fraction nevertheless decreases [17].

Figure 7 shows the annihilation time spectra for the ^4He runs with various levels of hydrogen impurity. These are normalized to the number of accepted antiprotons. For the comparison of Fig. 6 and Fig. 7, the binning of the time spectra was chosen to be 500 nsec. As the hydrogen impurity level increases, a marked change in the long lifetime component can be observed: even at 20 ppm H_2 concentration, the lifetime changes significantly. At 400 ppm impurity concentration, the long-lived compo-

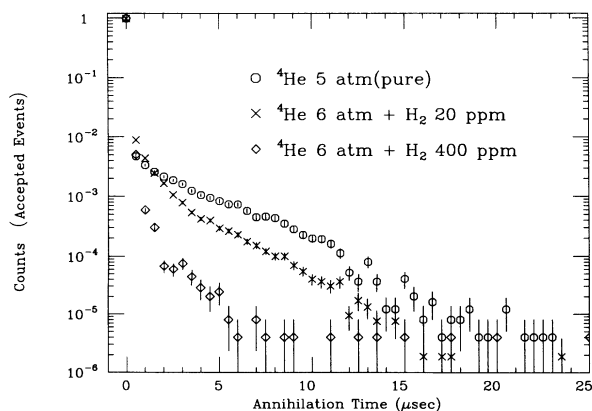


FIG. 7. Time spectra of pure ^4He and ^4He with H_2 impurity. Binning is 500 nsec per channel.

nent almost disappears. As for the trapping fraction, there seems to be no large difference among the various ^4He spectra, even with hydrogen impurities, which, as we have seen, strongly influence the trapping time. The trapping fraction for ^3He is nevertheless smaller than that for ^4He .

V. DISCUSSION

In the present experiment, we have established a method to observe delayed annihilation of \bar{p} in the gas target. We may summarize the implications of the experimental results as follows.

A. Similarity between gas and liquid

We successfully observed the delayed annihilation of antiprotons in gaseous ^4He as well as ^3He . The average lifetime in ^4He gases is about 3 μsec , which is very similar to the value obtained earlier in liquid helium at KEK [3]. The present observation clearly indicates two points. (1) When the delayed annihilation of antiprotons was discovered at KEK, it was not clear whether it was exclusively a characteristic of liquid helium or not. We have now established that the phenomenon exists in helium gas as well. (2) Contrary to our initial expectation, the time spectra and lifetimes are similar for liquid and gas in spite of the large difference in their densities. There is no theoretical estimate as to how strongly the metastability is affected by surrounding helium atoms.

B. Isotope effect

The average lifetime for ^3He is smaller by 15% than that for ^4He ($t_0 = 1 \mu\text{sec}$). The average lifetime depends on t_0 . Although the time spectrum cannot be represented by a single parameter, the spectra for ^4He and ^3He are very similar. This means that if we enlarge the time scale for ^3He by a suitable factor, the two spectra can approximately coincide, as shown in Fig. 8. In this way we can deduce an isotope ratio of the overall trapping time by the maximum likelihood method with the value

$$T_{\text{trap}}(^4\text{He})/T_{\text{trap}}(^3\text{He}) = 1.14 \pm 0.03.$$

This result is consistent with the theoretical model by Yamazaki and Ohtsuki [8], who on the basis of the Condo atomic model estimate the isotope effect to be roughly

$$\begin{aligned} T_{\text{trap}}(^4\text{He})/T_{\text{trap}}(^3\text{He}) &= [M^*(\bar{p} \ ^4\text{He})/M^*(\bar{p} \ ^3\text{He})]^2 \\ &= (16/15)^2 = 1.13, \end{aligned}$$

where M^* is the reduced \bar{p} mass. A similar value is obtained from the calculation which adopted a molecular approach to the $\bar{p}e^- \text{He}^{2+}$ system [9,10]. The difference in the trapping times comes from the difference of the level lifetimes and the level densities which depend on the reduced mass difference for $\bar{p} \ ^4\text{He}$ and $\bar{p} \ ^3\text{He}$. The agreement of the observed isotope ratio with the pre-

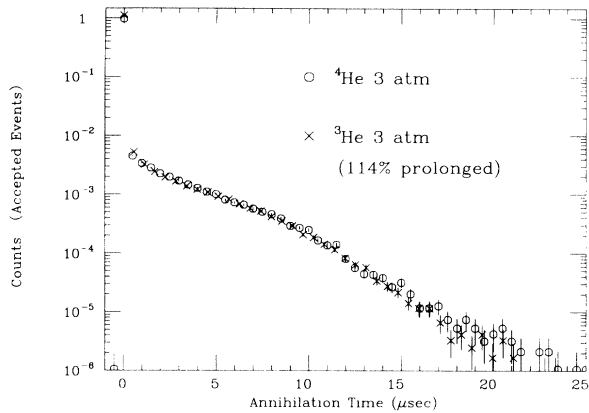


FIG. 8. Comparison of the time spectrum for ^4He (3 atm) with that for ^3He (3 atm) of which the time scale is enlarged by 14%. Binning is 500 nsec per channel.

diction supports the model of Condo for the metastability. However, the above estimate does not consider the \bar{p} slowing-down processes, the Auger transitions, and the quenching effects after the metastable-state formation. To obtain a more quantitative explanation for the isotope effect, theoretical studies of these processes are called for.

C. Quenching by impurity atoms or molecules

The long-lived delayed component is strongly suppressed by a small hydrogen contamination. Figure 9 shows the hydrogen-impurity dependence of $1/T_{\text{av}}$ with $t_0 = 100$ nsec. We can calculate the quenching cross section of hydrogen under the following assumptions: (1) the quenching takes place after the formation of metastable states and (2) the metastable-state system is thermalized after its formation in a time short compared with the annihilation time scale and hence its velocity v is thermal.

From these assumptions, we would expect a linear dependence of the annihilation rate λ on the impurity density n :

$$\lambda = \lambda_0 + \sigma_q v n,$$

where λ_0 is the intrinsic decay rate of the metastable state and σ_q is the quenching cross section. Here, we will use $1/T_{\text{av}}$ for λ .

The velocity of the $\bar{p}e^- \text{He}^{2+}$ system at room temperature is 1×10^5 cm/sec and that of H_2 is 1.5×10^5 cm/sec. The gradient of Fig. 9 is roughly 6×10^{-11} cm³/sec. This means $\sigma_q v = 6 \times 10^{-11}$ cm³/sec. Substituting v by 1.5×10^5 cm/sec, we obtain $\sigma_q \sim 4 \times 10^{-16}$ cm².

If we assume that the size of the $\bar{p}e^- \text{He}^{2+}$ system is

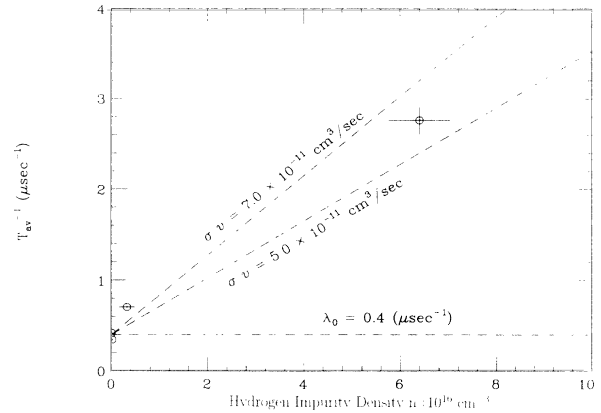


FIG. 9. Impurity dependence of T_{av}^{-1} for ^4He with H_2 .

similar to that of the helium atom and take the size of the hydrogen molecule to be twice that of the hydrogen atom, we estimate the geometrical collision cross section to be 4×10^{-16} cm². Thus the experimental quenching cross section is found to be the same as the geometrical cross section. This means that a single collision with a hydrogen molecule destroys the metastable state completely. There is no theoretical explanation for this effect. One or more of the previous assumptions might not be valid. It is an open question whether or not a small admixture of atoms or molecules with an ionization energy different from that of helium could change the initial (n, l) distribution when a \bar{p} is trapped and result in a different time spectrum.

To understand these results fully, systematic studies of the impurity dependence with various types of gases and of the dependence on the helium density (temperature and pressure variation) are essential. Such experiments are in progress and preliminary results have been reported in [17,18].

ACKNOWLEDGMENTS

We would like to thank the efforts of the CERN-LEAR staff for providing us with the stable high-quality low-momentum antiproton beam. We also thank Professor A.D. Donnachie and Dr. P. Darrulat for continuous encouragement and Dr. K. Ohtsuki for theoretical discussions. We used a VAX computer system of UTMSL in off-line analysis. The present work is supported by the Grant-in-Aid for Scientific Research and International Scientific Research of the Japanese Ministry of Education, Science and Culture and the International Joint Research Project of the Japan Society for the Promotion of Science. Support by the German Ministry of Research and Technology is also acknowledged. Two of the authors (S.N.N. and E.W.) acknowledge the receipt of support from JSPS.

- [1] S.N. Nakamura, M. Iwasaki, H. Outa, R.S. Hayano, Y. Watanabe, T. Nagae, T. Yamazaki, H. Tada, T. Numao, Y. Kuno, and R. Kadono, *Phys. Rev. A* **45**, 6202 (1992).
- [2] T. Yamazaki, M. Aoki, M. Iwasaki, R.S. Hayano, T. Ishikawa, H. Outa, E. Takada, H. Tamura, and A. Sakaguchi, *Phys. Rev. Lett.* **63**, 1590 (1989).
- [3] M. Iwasaki, S.N. Nakamura, K. Shigaki, Y. Shimizu, H. Tamura, T. Ishikawa, R.S. Hayano, E. Takada, E. Widmann, H. Outa, M. Aoki, P. Kitching, and T. Yamazaki, *Phys. Rev. Lett.* **67**, 1246 (1991).
- [4] G.T. Condo, *Phys. Lett.* **9**, 65 (1964).
- [5] J.E. Russell, *Phys. Rev. Lett.* **23**, 63 (1969); *Phys. Rev.* **188**, 187 (1969); *Phys. Rev. A* **1**, 721 (1970); **1**, 735 (1990); **1**, 742 (1970); *J. Math. Phys.* **12**, 1906 (1971); *Phys. Rev. A* **6**, 2488 (1972).
- [6] R.S. Hayano, M. Iwasaki, and T. Yamazaki, *Perspectives of Meson Science*, edited by T. Yamazaki, K. Nakai, and K. Nagamine (North-Holland, Amsterdam, 1992), Chap. 13.
- [7] R. Ahlrichs, O. Dumbrajs, H. Pilkuhn, and H.G. Schlaile, *Z. Phys. A* **306**, 297 (1982).
- [8] T. Yamazaki and K. Ohtsuki, *Phys. Rev. A* **45**, 7782 (1992).
- [9] I. Shimamura, *Phys. Rev. A* **46**, 3776 (1992).
- [10] P.T. Greenland and R. Thürwächter, *Hyperfine Interact.* **76**, 355 (1993).
- [11] T. Yamazaki, E. Widmann, R.S. Hayano, M. Iwasaki, S.N. Nakamura, K. Shigaki, F.J. Hartmann, H. Daniel, T. von Egidy, P. Hofmann, Y.-S. Kim, and J. Eades, *Nature (London)* **361**, 238 (1993).
- [12] J.F. Janni, *At. Data Nucl. Data Tables* **27**, 344 (1982).
- [13] H.H. Andersen and J.F. Ziegler, *Hydrogen Stopping Powers and Ranges in all Elements* (Pergamon, New York, 1977).
- [14] H.H. Andersen, in *Semiclassical Description of Atomic and Nuclear Collisions*, edited by J. Bang and J. de Boer (Elsevier Science, New York, 1985).
- [15] R. Medenwaldt, S.P. Møller, E. Uggerhøj, T. Worm, P. Hvelplund, H. Knudsen, K. Elsener, and E. Morenzoni, *Phys. Lett. A* **155**, 155 (1991).
- [16] P.V. Vavilov, *Zh. Eksp. Teor. Fiz.* **32**, 920 (1957) [*Sov. Phys. JETP* **5**, 749 (1957)].
- [17] OBELIX Collaboration, *Nucl. Phys. A* **558**, 665c (1993).
- [18] E. Widmann, H. Daniel, J. Eades, T. von Egidy, F.J. Hartmann, R.S. Hayano, W. Higemoto, J. Hoffmann, T.M. Ito, M. Iwasaki, A. Kawachi, N. Morita, S.N. Nakamura, N. Nishida, W. Schmid, I. Sugai, H. Tamura, and T. Yamazaki, *Nucl. Phys. A* **558**, 679c (1993).

